Appl. Phys. B 73, 523–529 (2001)
DOI: 10.1007/s003400100670

Applied Physics B
Lasers and Optics

A. ROSENFELDT
M. FLÖRSHEIMER✉

Nondestructive remote imaging of ferroelectric domain distributions with high three-dimensional resolution

Physical Institute, University of Münster, Wilhelm-Klemm-Straße 10, 48149 Münster, Germany

Received: 16 May 2001
Published online: 23 October 2001 • © Springer-Verlag 2001

ABSTRACT The domain distribution in the bulk and at the surface of ferroelectric crystals is imaged by second-harmonic microscopy with three-dimensional far-field optical resolution. The nondestructive technique allows us to investigate the success of a poling procedure in a fabrication state of an integrated optical device in which the poling electrodes have not been removed. Additionally, a confocal linear optical imaging technique is introduced, which reveals the surface topography with ± 0.7 nm height sensitivity. At the surface of a periodically poled specimen, we detect unexpected and unwanted surface topographies that correspond to the domain structure. The search for improved fabrication parameters that guarantee smooth surfaces could be substantially promoted with our topography-detection technique.

PACS 07.60.Pb; 42.70.Mp; 42.79.Sz; 42.82.Bq; 78.68.+m; 81.70.Fy

1 Introduction

Ferroelectric materials are applied in various electro-optic, acousto-optic, and nonlinear optical devices, for example, as modulators of light, optical frequency converters or tunable sources of coherent light for spectroscopic applications [1, 2]. Also, the optical functionality of ferroelectrics can be integrated monolithically with optical waveguides. Such integrated optical devices enable the optical Internet and its continuous growth. Additionally, ferroelectrics are highly interesting for the development of nonvolatile, fast, random-access memories [3]. For all these applications, the control and knowledge of the ferroelectric domain distribution in a crystal are essential. Recently, we have developed a simple, nondestructive nonlinear optical imaging technique [4], which allows us to observe the ferroelectric domain boundaries with three-dimensional far-field optical resolution. No sample preparation is required. Here, we apply this technique to periodically poled $LiTaO_3$ (PPLT) specimens. Additionally, we show that the same microscope can be used in a linear optical mode of operation in order to image the surface topography of the samples with ± 0.7 nm height sensitivity.

✉ Fax: +49-251/83-33602, E-mail: florshl@nwz.uni-muenster.de

2 Experimental

A confocal laser scanning microscope (Leica Aristoplan CLSM) with oil-immersion objectives (40x/numerical aperture $NA = 1.30$ and $100\text{x}/NA = 1.32$) was used. The microscope was operated in a nonlinear [4] and a linear optical mode of imaging. In both cases, laser light was tightly focused by means of the objective. The focal spot was then scanned line-wise across the object plane using galvanometer mirrors. The axial position of the focus relative to the sample could be altered by an axial translation of the stage that supported the sample. The light source in the linear optical experiments was a continuous-wave argon-ion laser (Leica Omnichrome). The light at a wavelength of $\lambda = 488$ nm reflected from the surface of the sample was collected with the objective and detected using a confocal pinhole and a photomultiplier. An optical section could be recorded within a time of 1 s. Typical images used here, however, are an average over 60 scans of the same section. This average was taken in order to reduce noise, which originated from imperfectly damped mechanical vibrations of the microscope.

For the nonlinear optical studies, a mode-locked Ti:sapphire laser (Coherent Mira) was used. By means of an autocorrelator (NT&C, Marnheim, Germany), we determined the time duration of the pulses after passing through the microscope to be $\backsim 400$ fs. Due to the short pulses, high focal intensities could be applied without damaging the specimens. The PPLT samples were probed with pulse intensities in the order of 4×10^{10} W/cm^2 at a repetition rate of 76 MHz and a wavelength of $\lambda = 800$ nm. The ferroelectric material in the laser focus generated a second-harmonic (SH) signal. The backwards-radiated SH intensity was then measured without a detection pinhole [5]. For the separation of the SH signal in the microscope from backwards-scattered fundamental light, a harmonic beam splitter (650 DCSPXR, AF Analysentechnik, Tübingen, Germany) and a color glass filter (BG 18, Schott, thickness 3 mm) were used. The recording times for the SH images shown here were between 4 and 6 min.

The results obtained with the optical techniques were compared with atomic force micrographs of the sample surfaces. Topographic images were taken using the tapping mode of a NanoScope III/Dimension 3000 force microscope (Digital Instruments). Rectangular silicon cantilevers (Nanosensors, Wetzlar, Germany) with a nominal length of 123 μm and

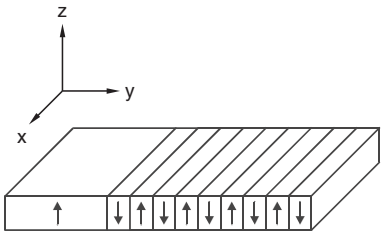

FIGURE 1 Schematic geometry of the investigated specimens. The dipoles of the ferroelectric domains are indicated with *arrows*. No surface topography is expected

a resonance frequency in the range between 313 and 389 kHz were applied.

The PPLT samples were obtained from Jan-Peter Meyn, University of Kaiserslautern. Six Z-cut specimens with poling periods between $\Lambda = 4.65\,\mu\text{m}$ and $\Lambda = 20\,\mu\text{m}$ were studied. Here, we show results from two typical examples with poling periods of $\Lambda = 8\,\mu\text{m}$ and $\Lambda = 4.65\,\mu\text{m}$, respectively. The coordinates indicated in the images below correspond to the crystallographic axes of the specimens. Figure 1 schematically shows the geometry of the samples. They were not etched. No surface topography is expected. The probing light in the optical experiments was preferentially polarized parallel to the x axis of the specimens.

3 Second-harmonic imaging

3.1 *Phenomena and interpretation*

Figure 2 shows a z/y scan of the sample with $\Lambda = 8\,\mu\text{m}$. In the experiment, the objective was above the specimen. The axis of the objective was parallel to the crystallographic z axis. In the image, we look at the surface and into the bulk of the sample below the surface. A bright stripe near the top of the image and a series of additional bright lines parallel to the z axis can be seen. The stripe near the top of the micrograph corresponds to the sample surface; the other lines can be identified with the walls between the periodically inverted domains.

So far, we have no quantitative theory for the contrast. In a recent study of $LiNbO_3$ specimens, however, we observed similar phenomena and proposed the following interpretation [4]: in our geometry where we apply a tightly focused laser beam and detect the backwards-scattered harmonic light, the coherence length for the nonlinear process is small. For $LiNbO_3$, we calculated it to be 43 nm [4], which is much smaller than the Rayleigh range of the laser focus. Thus a signal is radiated from a thin film just below the surface, whose thickness corresponds to the coherence length. If the focus is moved downwards into a homogeneous bulk region, the SH waves interfere mainly destructively. Thus, the homogeneous bulk material appears dark. At the domain walls, however, the linear or nonlinear properties of the material are disturbed, which changes the phase-matching conditions and makes the walls visible. Similar contrasts and explanations were also given in recent third-harmonic imaging studies of centrosymmetric specimens [6, 7].

The axial width (full width at half maximum) of our surface signal is $\Delta s = 1100 \pm 100\,\text{nm}$. The lateral width of the signal from the domain walls is $\Delta s' = 310 \pm 30\,\text{nm}$. These widths correspond to the axial and lateral resolutions of the microscope. The SH intensity from the domain walls is maximum for a depth in the order of 10 μm below the surface. If the laser focus is moved upwards or downwards from this optimum position the SH intensity decreases. At the surface, the signal from the walls is smaller as compared to the surface signal. This phenomenon can be observed particularly well in Fig. 3, which gives a section in the z/y plane near the surface of the same sample as in Fig. 2 but with higher magnification.

The intensity change of the wall signal with increasing depth of the laser focus below the surface is probably due to the change of the focus parameters with depth. The objective is corrected for a material with the refractive index $n = 1.518$ of the immersion oil. In such a material, the minimum focus size is obtained. In matter with higher refractive indices [8], such as our ferroelectric samples, the axial and lateral focus sizes become larger. Additionally, these parameters increase with depth. We can assume that the highest SH intensity is obtained in a depth where the beam parameters correspond to optimum phase matching.

Figures 4 and 5 show the $+Z$ and the $-Z$ faces of the sample, respectively (x/y scan). In the two surface images, the domain walls can be seen as dark lines. Additionally, we observe a slight difference in the SH intensities from the surfaces of the inversely oriented domains in Fig. 4 and 5. This phe-

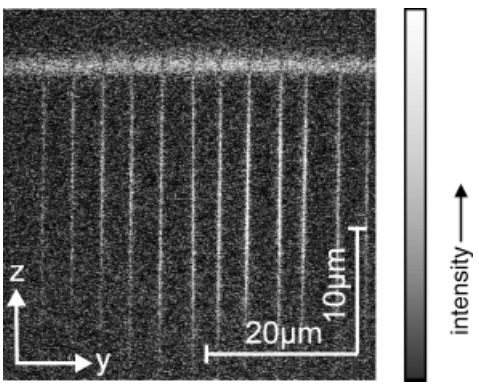

FIGURE 2 Second-harmonic image of a section in the z/y plane of the sample with $\Lambda = 8\,\mu\text{m}$. The surface and the domain walls in the bulk below the surface can be seen

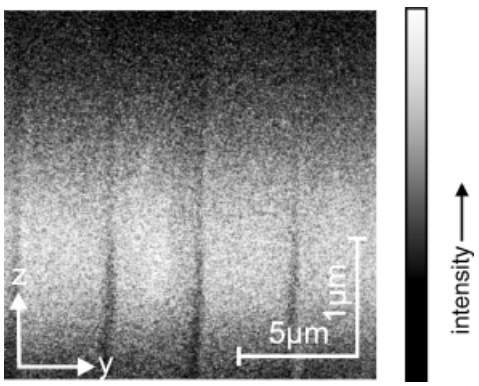

FIGURE 3 Section in the z/y plane near the surface of the same sample as in Fig. 2 ($\Lambda = 8\,\mu\text{m}$) but with higher magnification

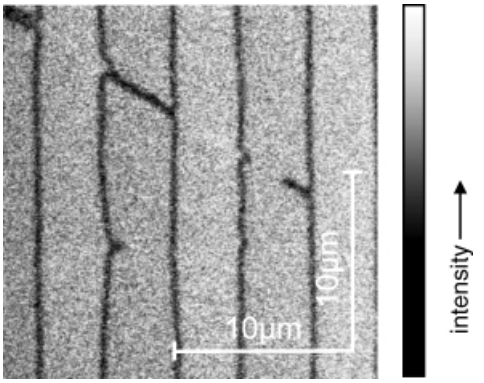

FIGURE 4 Second-harmonic image of the $+Z$ face of the sample with $\Lambda = 8\,\mu$m, x/y scan

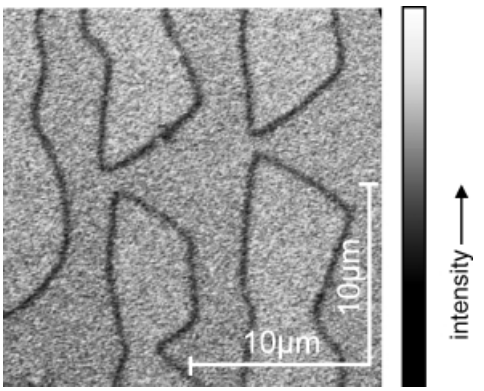

FIGURE 5 Second-harmonic image of the $-Z$ face of the sample with $\Lambda = 8\,\mu$m, x/y scan

nomenon has also been observed with $LiNbO_3$ samples by the integrated optics group in Paderborn [9]. The contrast may be due to (i) a different roughnesses; (ii) different contaminations or (iii) different heights of the alternating domains. The answer will be given in the linear optical studies below.

In Fig. 6, two regions at the $+Z$ face of the sample with $\Lambda = 4.65\,\mu$m are shown. The bright spots and lines are remainders of metal electrodes that had been evaporated for the poling procedure. Figure 6a is typical for the main part of the surface. The dark strips are the walls between the neighboring domains. In this surface section, the periodic inversion of the ferroelectric polarity was successful although the domain width is not very homogeneous. In another part (Fig. 6b), however, the poling procedure failed.

3.2 *Discussion*

Although we have not quantitatively verified our model of the contrast so far, we can apply our SH imaging technique for the nondestructive investigation of ferroelectric domain distributions. Figure 6 shows that we can even see the domain structure in a state where the poling electrodes have not been removed. In such a state, additional attempts to pole the crystal are possible. In contrast, the conventional technique, selective etching, is a destructive method, which makes a second attempt at poling very difficult.

In addition to the distribution of the domains at the surfaces, our nonlinear microscope also reveals the ferroelectric domain structure in the interior of bulk samples with three-

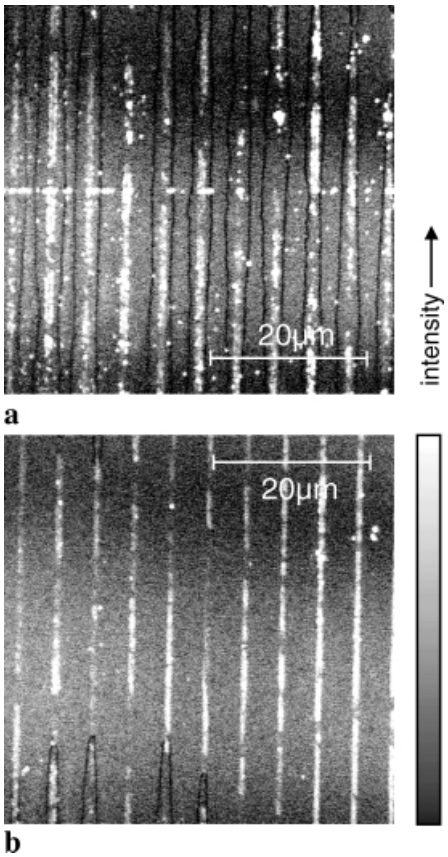

FIGURE 6 Second-harmonic images of two regions at the $+Z$ face of a sample with remainders of poling electrodes (x/y scans, $\Lambda = 4.65\,\mu$m). In a part of the surface **a**, the domain inversion was successful. In another part **b**, the poling procedure failed

dimensional far-field optical resolution. This information is not obtained with any other simple technique [4]. A high impact of SH imaging on the further development of ferroelectric devices, on the control of fabrication processes and on the quality control of crystals and integrated optical devices is expected.

4 Linear optical imaging

4.1 *Topography detection from two-dimensional scans*

In our linear optical experiments, the domain walls in the bulk of the samples could not be seen. The linear optical scanning confocal microscope, however, can be used to measure the topography and to detect defects at the surface with high sensitivity. A simple method for surface profiling, based on the two-dimensional (2D) scanning of a sample, was introduced recently [10, 11]. We first describe this technique. Then, we improve it and apply it to ferroelectric specimens.

The principle of the 2D scanning method is illustrated in Fig. 7. The focus of a laser beam is moved over a sample surface at constant height. The part of the reflected light that is collected from the objective can be measured. Due to the topography of the specimen in the example of Fig. 7, the distance between focus and surface is altered during the 2D scan. The change of the distance influences the measurable signal. Sensitive light detection allows us to determine fine topographical details of the surface. Figure 8 gives the theor-

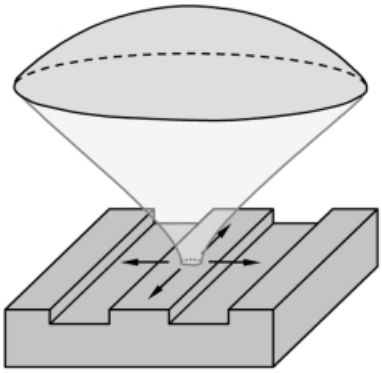

FIGURE 7 Principle of surface-topography detection from a two-dimensional scan of a sample at constant height of the laser focus. The part of the reflected light that is collected from the objective can be measured in the microscope. Slight changes of the focus/surface distance influence the collected signal. From precisely measured intensities, fine topographical details can be calculated

etical intensity response I of the microscope as a function of the distance Δz between the center of the focus and the surface. The intensity is a maximum for $\Delta z = 0$ and decreases symmetrically if the focus is moved upwards (Δz positive) or downwards (Δz negative). The half width Δs of the central peak is a measure of the microscope's axial resolution. Two interfaces of a specimen whose optical distance is smaller than Δs will be difficult to distinguish.

Optical profiling, however, allows us additionally to detect fine height changes at a surface whose dimensions are far below the resolution limit. In order to obtain the optimum sensitivity for small height changes, the microscope must be operated at the steepest slope dI/dz of its response curve (see Fig. 8). In an experiment, the height of the focus must hence be adjusted such that Δz is near the optimum working distance during the whole 2D scan. The height sensitivity σ_z of the technique can be given as [11]

$$\sigma_z = \left|\frac{\mathrm{d}z}{\mathrm{d}I}\right| \sigma_I \qquad (1)$$

where σ_I is the noise level of the measured intensity.

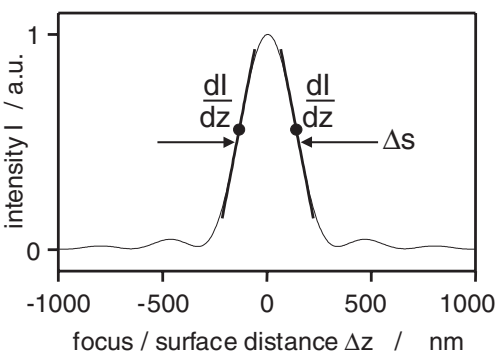

FIGURE 8 Calculated reflected light intensity I behind the detection pinhole of a confocal microscope ($NA = 1.30$, $\lambda = 488$ nm) as a function of the axial distance Δz between laser focus and surface. The half width Δs of the main peak is a measure of the microscope's resolution. Additional fine topographical details far below the resolution limit can be obtained from precise intensity measurements if the microscope is operated in the regions of the steepest slope dI/dz in the response curve. The positions of optimum working distance are indicated

In Fig. 8, we calculated the intensity I of the reflected light that passes through the confocal detection pinhole of our microscope by using an electromagnetic theory [12], in which the phase fronts of the probing light after the objective are considered as spherical waves in order to account for wide angular apertures (no paraxial approximation). The curve in Fig. 8 was obtained for an objective with $NA = 1.30$ and a wavelength of $\lambda = 488$ nm. The diameter of the pinhole was set to be so small that an additional reduction of its size does not reduce the width of the main peak additionally. The theoretical resolution obtained in this case is $\Delta s = 297$ nm.

The sensitivity of the microscope for additional fine topographical details below the resolution can be estimated as follows: in our example, the slope of the response curve at the optimum working distance Δz_w can be determined to be $|\mathrm{d}I/\mathrm{d}z|\,(\Delta z_w) = I_{\max}/199\mathrm{nm}$ with $I_{\max}$ the maximum intensity at $\Delta z = 0$. We may assume a standard deviation of the noise in an experiment of 1% relative to the measured intensity. If we then approximate the intensity at the working distance to be $I_{\max}/2$, we obtain a sensitivity of $\sigma_z \backsim (199\mathrm{nm}/I_{\max})(0.01 I_{\max}/2) = 1\mathrm{nm}$. Additionally, we can estimate the maximum height changes in a surface that are measurable in a 2D scan. With increasing and with decreasing height of a surface detail relative to the optimum position, the sensitivity of the microscope is reduced. We may allow an increase of σ_z by a factor of two as compared to the optimum sensitivity, which corresponds to an increase of the slope $|\mathrm{d}z/\mathrm{d}I|$ in Eq. (1) also by a factor of two. This slope is obtained at intensities of 94 and 11% of the maximum response in Fig. 8. A height difference of 199 nm corresponds to this intensity range.

4.2 *Improvement of the topography detection and application of the method*

So far, we have considered 2D scans of a surface. Below, we improve the topographical sensitivity by scanning additionally into the depth of the material. Using such a 3D method, we can measure the complete axial intensity profile for any surface point of a specimen. From the measured axial profile, we then calculate the height position of the corresponding surface site. Figure 9 shows an example of a z/y scan through the $+Z$ surface into the depth of the PPLT sample with $\Lambda = 8\,\mu$m. The surface signal is axially broadened as expected. Additionally, a lateral structure with the periodicity of the ferroelectric domains can be seen. An axial intensity profile is given on the right-hand side of Fig. 9. It was taken from the middle domain in Fig. 9 at the solid line indicated there.

The width of the profile is $\Delta s = 430$ nm, corresponding to the axial resolution of the microscope. This value is not as good as the theoretical resolution ($\Delta s = 297$ nm) which, however, was calculated for a perfect microscope. Also, the shapes of the real and the calculated intensity profile differ from each other. In the real microscope, the intensity response is not perfectly symmetric. If the laser focus in the experiment is below the surface, the measured response curve is steeper as compared to the case of the focus above the surface. Using the real microscope for topography detection in a 2D x/y scan, the optimum height of the focus is thus below the sample surface. This optimum working height is indicated in Fig. 9 with a broken line.

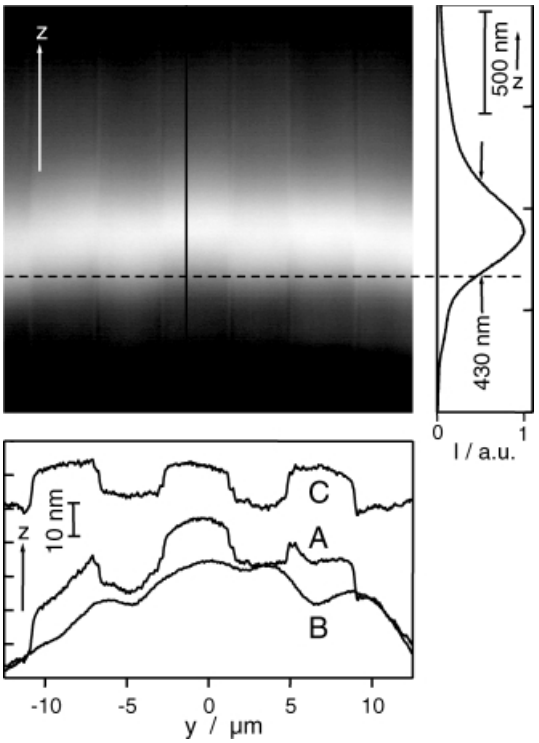

FIGURE 9 Linear confocal image of a section in the z/y plane of the sample with $\Lambda = 8\,\mu$m together with an axial intensity profile and the calculated height profiles. The ferroelectric domain structure of this sample is accompanied with a topography. The intensity profile corresponds to the line indicated at the middle domain of the image. The intensity profiles of the neighboring domains are axially shifted with respect to each other. The topographical cross-section A was calculated from the image, curve B describes the background and curve C gives the background-corrected topography profile

In the z/y scan of Fig. 9, the axial intensity profiles from the neighboring domains are vertically shifted with respect to each other. This phenomenon indicates steps at the surface. In order to calculate the topography we could fit all the measured axial profiles with a model. From the fits, we could determine the height position of the maximum intensity for any profile. This maximum is expected to correspond with the height of the surface. The theory given above, however, does not account for the imperfections of the real imaging system. Hence, we used an alternative method for the calculation of the topography. From the axial intensity profiles, we determined an expectation value $\langle z\rangle$ of the surface according to

$$\langle z\rangle(x, y) = \int_{-\infty}^{+\infty} I(x, y, z)z\mathrm{d}z \Big/ \int_{-\infty}^{+\infty} I(x, y, z)\mathrm{d}z\,. \qquad (2)$$

The result of this calculation for the z/y scan in Fig. 9 is given as curve A below the image.

After we had taken the data we imaged four other surface sections of the same sample under identical conditions as compared to the image of Fig. 9. In these sections, no inverted domains had been written into the crystal. Curve B in Fig. 9 is the calculated height profile averaged over the four sections. The four individual curves were identical except for the noise that became reduced in the averaging procedure. We can thus conclude that the surface sections without inverted domains are topographically flat. The profile in curve B is due to scanning artifacts of the microscope. While moving the focus horizontally its height position does not remain perfectly constant. Since curve B, however, is reproducible we can subtract it from curve A as a topographical background. The result is curve C. This profile shows that the ferroelectric domain structure of this sample is accompanied by a significant surface topography. Step heights between adjacent domains in the order of 10 nm are observed.

4.3 *Discussion of the observed topography*

The topography revealed in the example of the specimen with $\Lambda = 8\,\mu$m explains the slight contrast in the SH intensities between the inverted domains observed in Fig. 4 and 5. Nevertheless, the existence of a topography at this surface is highly astonishing because the sample was not etched. The inversion of the ferroelectric polarity could explain topographical steps in the order of the lattice constants or much less but not in the order of 10 nm. Probably, the topography is due to unwanted and uncontrolled chemical reactions that took place during or after the chemical removal of the poling electrodes. In the fabrication of waveguide and integrated optical devices, such processes must be avoided. The surfaces of waveguides must be smooth and free of defects, which would give rise to attenuation losses of guided modes of light. The possibility to observe unwanted topographies with a simple microscope, however, could be used to control and to improve the fabrication processes.

4.4 *Determination of the topographical sensitivity obtained in two- and three-dimensional scanning modes*

The height sensitivity of the microscope is limited by the noise in the calculated topographies. In Fig. 10, two height profiles with different noise are compared. One profile is the reproduced curve C of Fig. 9 (3D scanning technique).

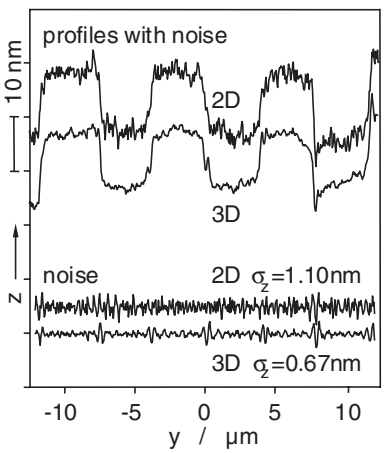

FIGURE 10 Height sensitivity of the linear confocal scanning methods. The topographical profiles were calculated from the image of Fig. 9 by applying the three-dimensional (3D) and an improved two-dimensional (2D) detection technique. The height sensitivity is limited by the noise in the curves. After Fourier filtering, the high spatial frequency fluctuations in the profiles were obtained. The standard deviations σ_z of these fluctuations are given for the two techniques

The other profile was calculated for the same image but in this case we used only a part of the information in the axial intensity distribution (modified 2D technique). We calculated the average intensities in an interval of focus/surface distances around the optimum height for 2D scanning. The size of the interval was ±20 nm. We expect that the noise level in the topography obtained from the 3D method is smaller as compared to the noise in the data from the 2D technique. Comparing the two profiles in Fig. 10, we can see, in actual fact, that the fluctuations at high spatial frequencies are smaller for the 3D method.

In order to extract the noise from the profiles, we Fourier-filtered the high frequencies (transmission for spatial frequencies $\tilde{v} \geq 1/700\text{nm}$). The resulting curves are given in the lower part of Fig. 10. For a first estimation of an upper limit for the noise level, we considered the fluctuations in these curves to be only due to noise and not to topographical details at high spatial frequencies. We then calculated the standard deviations of the fluctuations and scaled them to the full bandwidth of our microscope's A/D converter, which takes 512 samples per line scan. The results are $\sigma_z = 1.1$ nm for the 2D method and $\sigma_z = 0.67$ nm for the 3D technique. The latter standard deviation corresponds to only 0.14% of the wavelength of the probing light used.

The main source of noise in our experiments was mechanical vibrations of the microscope. Also, the laser used for the measurements exhibited intensity fluctuations of more than ±2%. Great additional improvements of the height sensitivity should be easily achievable with a better pneumatic vibration isolation and with intensity-stabilized lasers.

4.5 *Discussion of the two topography detection techniques*

Above, we have shown that the sensitivity of the 3D technique is superior to the 2D method as was expected. Another advantage of the 3D technique is that the maximum height differences in a surface that can be detected are not limited by the size of the laser focus as in the case of the 2D technique. Above, we have shown that the latter method is restricted to surfaces with height variations of a few hundred nm. A third benefit of the 3D technique is that it allows us to distinguish materials and topographic contrasts. Materials with different refractive indices exhibit different reflectivities. Thus, the absolute intensities of the reflected light are influenced by the chemical composition, whereas height changes at a surface lead to an axial shift of the intensity profiles. Details will be investigated in a future paper. If the topographic sensitivity, the applicability to marked height changes and the chemical selectivity of the 3D method are not needed, the 2D technique can be favorably applied because the time required for data acquisition in this case is shorter as compared to the time for a full 3D scan of a specimen's surface region.

Our 3D method to determine the position of a surface from axial intensity profiles with high sensitivity is closely related to single-molecule detection [13] with far-field optical microscopes. Of course, individual molecules cannot be resolved with such instruments. This means that a magnified copy of a molecule with its original shape cannot be obtained. Nevertheless, single molecules can be detected, for example, if they are fluorescent. In an image, taken with a confocal fluorescence microscope, a molecule then appears as a spot of fluorescence light whose dimensions are given by the resolution of the microscope. The intensity profiles of the spot can be analyzed in a similar way as the axial intensity profiles from our surfaces. From the fluorescent spot profiles, the position of the molecule can be determined with a precision of a few tens of nm. This method allows us, for example, to observe the motion of individual functional molecules such as proteins in solution or in a living cell [14].

In our topography-detection experiments, we have, however, to consider additionally that the lateral resolution is much lower as compared to the axial sensitivity. Thus, the calculated topography may not be a perfect copy of the original surface. The comparison of the two profiles in Fig. 10, which were calculated from the same surface with different techniques, indicates also that such limitations of the method must be discussed. The profiles in Fig. 10 obtained with the 3D method look more rounded as compared with the curves calculated with the 2D technique. We thus compare our results with atomic force micrographs.

5 Surface imaging by atomic force microscopy and comparison with the optical topography-detection techniques

A topographical image from the specimen with $\Lambda = 8$ μm obtained with the atomic force microscope (AFM) is given in Fig. 11. A time of ∽10 min was required to take the image. The fast scanning direction of the AFM was roughly parallel to the crystallographic y axis. Marked periodic height changes are observed while scanning parallel to this direction. The periodicity corresponds to the poling period of the sample. The height differences are in the same order of 10 nm as calculated from the linear optical images. The edges of the profiles are rounded. This phenomenon is no artifact, as was verified by scanning the surface with different speeds and at different length scales. The height change in the image of Fig. 11 alongside the slow scanning direction, however, is

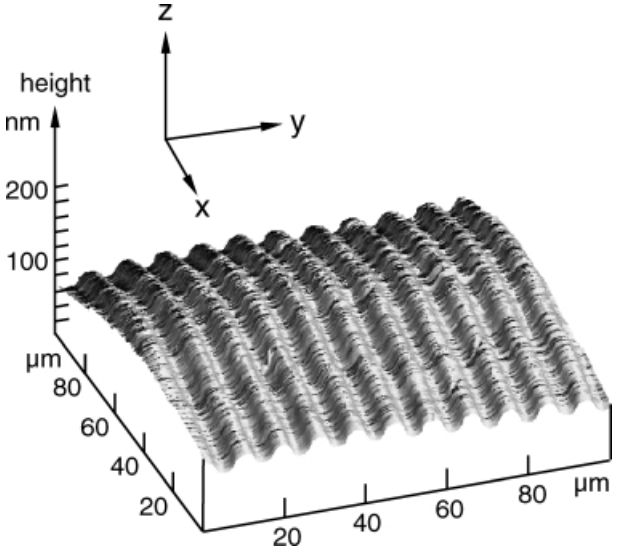

FIGURE 11 Topographical image of the sample with $\Lambda = 8$ μm obtained by atomic force microscopy

not due to a real topography. During the time required for the acquisition of the image from a large area as in Fig. 11, drift in the piezo element of the AFM occurs.

The lateral resolution of the AFM is superior to the lateral resolution of our far-field optical microscopes. The AFM, however, is particularly useful for the investigation of small surface sections. If large areas such as the surfaces of ferroelectric devices must be investigated, the optical 2D scanning technique can save much time. The optical 3D technique is particularly useful if high height sensitivity is important and the exact two-dimensional shape of the surface features is of minor interest. In device-fabrication processes where the kind and shape of possible defects are known, such an optical technique may be beneficial in order to detect the existence of an unwanted feature reliably but not its shape. An additional benefit of the optical technique is that the same microscope can be used in its nonlinear mode of operation in order to image the ferroelectric domain structure of the specimen up to large depths below the surface.

6 Conclusion

A laser scanning microscope was used to characterize PPLT specimens. In a nonlinear optical mode of imaging, the ferroelectric domain distribution was revealed at the surface and in the bulk of the crystals at depths of up to several tens of μm. The nondestructive technique can be used, for example, to control the success of a poling procedure in a state of the sample where the electrodes have not been removed.

An additional linear optical mode of imaging was introduced which allowed us to detect the surface topography of the specimens with a height sensitivity of $\Delta z = \pm 0.7$ nm. Applying this method, we observed that ferroelectric domain structures were accompanied with unexpected and unwanted surface topographies. In contrast, the surfaces of waveguides in integrated optical devices should be smooth and free of defects in order to avoid attenuation losses of guided modes. Our topography-detection technique could help to identify optimum processing parameters for integrated optical devices with smooth surfaces.

ACKNOWLEDGEMENTS We would like to thank J.-P. Meyn, Kaiserslautern, for the specimens. Useful discussions on ferroelectric materials with D. Hofmann, G. Schreiber and W. Sohler, Paderborn, are also gratefully acknowledged. The AFM image was taken by L.-F. Chi, Münster. Financial support was obtained from the Volkswagen Foundation and the Federal Ministry for Schools, Advanced Education, Science and Research of Northrhine-Westfalia.

REFERENCES

1 B.E.A. Saleh, M.C. Teich: *Fundamentals of Photonics* (Wiley, New York 1991)
2 M.M. Fejer: Phys. Today **47**, 25 (1994)
3 O. Auciello, J.F. Scott, R. Ramesh: Phys. Today **51**, 22 (1998)
4 M. Flörsheimer, R. Paschotta, U. Kubitscheck, C. Brillert, D. Hofmann, L. Heuer, G. Schreiber, C. Verbeek, W. Sohler, H. Fuchs: Appl. Phys. B **67**, 593 (1998)
5 W. Denk, J.H. Strickler, W.W. Webb: Science **248**, 73 (1990)
6 M. Müller, J. Squier, K.R. Wilson, G.J. Brakenhoff: J. Microsc. **191**, 266 (1998)
7 D. Yelin, Y. Silberberg: *Eur. Microsc. Anal.* 13, Nov. (2000)
8 S. Hell, G. Reiner, C. Cremer, E.H.K. Stelzer: J. Microsc. **169**, 391 (1993)
9 D. Hofmann, G. Schreiber, W. Sohler (Paderborn): personal communication
10 C.-H. Lee, J. Wang: Opt. Commun. **135**, 233 (1997)
11 M. Bender: Diploma thesis, Marburg (1999)
12 C.J.R. Sheppard, J. Felix Aguilar: Opt. Commun. **180**, 1 (2000)
13 N. Bobroff: Rev. Sci. Instrum. **57**, 1152 (1986)
14 U. Kubitscheck, O. Kückmann, T. Kues, R. Peters: Biophys. J. **78**, 2170 (2000)